Circulation Research

Volume 129, Issue 7, 17 September 2021; Pages 751-766 https://doi.org/10.1161/CIRCRESAHA.120.317076



ORIGINAL RESEARCH

Filamin C Cardiomyopathy Variants Cause Protein and Lysosome Accumulation

Meet the First Author, see p 701

Radhika Agarwal, Joao A. Paulo , Christopher N. Toepfer , Jourdan K. Ewoldt, Subramanian Sundaram , Anant Chopra, Qi Zhang, Joshua Gorham , Steven R. DePalma , Christopher S. Chen, Steven P. Gygi*, Christine E. Seidman *, and J.G. Seidman *

RATIONALE: Dominant heterozygous variants in filamin C (*FLNC*) cause diverse cardiomyopathies, although the underlying molecular mechanisms remain poorly understood.

OBJECTIVE: We aimed to define the molecular mechanisms by which *FLNC* variants altered human cardiomyocyte gene and protein expression, sarcomere structure, and contractile performance.

METHODS AND RESULTS: Using CRISPR/Cas9, we introduced *FLNC* variants into human induced pluripotent stem cell–derived cardiomyocytes (hiPSC-CMs). We compared isogenic hiPSC-CMs with normal (wild-type), ablated expression ($FLNC^{-/-}$), or haploinsufficiency ($FLNC^{+/-}$) that causes dilated cardiomyopathy. We also studied a heterozygous in-frame deletion ($FLNC^{+/\Delta 7aa}$) which did not affect FLNC expression but caused aggregate formation, similar to FLNC variants associated with hypertrophic cardiomyopathy. $FLNC^{-/-}$ hiPSC-CMs demonstrated profound sarcomere misassembly and reduced contractility. Although sarcomere formation and function were unaffected in $FLNC^{+/-}$ and $FLNC^{+/\Delta 7aa}$ hiPSC-CMs, these heterozygous variants caused increases in lysosome content, enhancement of autophagic flux, and accumulation of FLNC-binding partners and Z-disc proteins.

CONCLUSIONS: FLNC expression is required for sarcomere organization and physiological function. Variants that produce misfolded FLNC proteins cause the accumulation of FLNC and FLNC-binding partners which leads to increased lysosome expression and activation of autophagic pathways. Surprisingly, similar pathways were activated in *FLNC* haploinsufficient hiPSC-CMs, likely initiated by the loss of stoichiometric FLNC protein interactions and impaired turnover of proteins at the Z-disc. These results indicate that both *FLNC* haploinsufficient variants and variants that produce misfolded FLNC protein cause disease by similar proteotoxic mechanisms and indicate the therapeutic potential for augmenting protein degradative pathways to treat a wide range of *FLNC*-related cardiomyopathies.

Key Words: cardiomyopathies ■ filamin ■ induced pluripotent stem cell ■ lysosome ■ sarcomere

* S.P. Gygi, C.E. Seidman, and J.G. Seidman contributed equally.

© 2021 American Heart Association, Inc.

Nonstandard Abbreviations and Acronyms

DCM dilated cardiomyopathy
DE differentially expressed

DES desmin

FBLIM1 migfilin/filamin binding LIM protein 1

FILIP1 filamin A interacting protein 1

FLNC filamin C

HCM hypertrophic cardiomyopathy

hiPSC human induced pluripotent stem cell

hiPSC-CMs human induced pluripotent stem cell-derived cardiomyocytes

HSP heat shock proteins

ITGB1 β1-integrin tail

MFM myofibrillar myopathy

MYOT myotilin

MYOZs myozenins

PDLIM3 PDZ and LIM domain 3

PGM5 aciculin

SGCG γ-sarcoglycan

SORBS costamere-associated protein

SYNPO2 synaptopodin 2

TTN titin

XIRPs xin proteins

ardiomyopathy, characterized by pathological cardiac enlargement and contractile dysfunction, is a leading cause of heart failure. Among patients with nonischemic cardiomyopathy, a cause is identified in over 20%, including damaging variants (loss of function, in-frame deletions/insertions, and deleterious missense) in over 40 genes with diverse functions in cardiomyocyte biology. These variants cause diverse forms of cardiac remodeling which are clinically subclassified into hypertrophic cardiomyopathy (HCM), dilated cardiomyopathy (DCM), and restrictive cardiomyopathies, among others. A critical next step to improve the understanding of human heart failure is to define shared and distinct mechanisms by which these variants cause disease.

Variants in *FLNC*, encoding filamin C, have emerged as a more common cause of cardiomyopathy.^{3–6} *FLNC* truncating variants are found in ≈3% to 4% of patients with DCM which

presents in early-to-mid adulthood and is associated with a high rate of ventricular arrhythmias and sudden cardiac death. 6–9 *FLNC* missense variants are more commonly associated with HCM and can cause pathological FLNC protein aggregation. 9 However, there is considerable overlap between the cardiomyopathy phenotypes caused by distinct classes of *FLNC* variants, with missense, splice site, and in-frame indels reported in DCM, HCM, and restrictive cardiomyopathy. 3,9,10

Filamins (FLNA, FLNB, FLNC) are dimeric proteins, consisting of 270 to 290 kDa subunits, that crosslink filamentous (F-) actin. 11,12 FLNs contain an N-terminal ABD (actin-binding domain) followed by 24 immunoglobulin-like repeats, the last of which mediates protein dimerization. 13,14 FLNC (Figure 1) is uniquely and highly expressed in cardiac and skeletal muscle 15,16 and has an immunoglobulin-like domain insertion that enables sarcomere binding at Z-discs, where it crosslinks actin to anchor thin filaments. 16 FLNC is less abundantly found at costameres (specialized focal adhesion complexes that connect sarcomeres to the sarcolemma) and at intercalated discs. 12,17,18 At these locations and at Z-discs, the C-terminal immunoglobulin domains (immunoglobulin 16–24) of FLNC interact with a large number of proteins with diverse structural and signaling roles, including the dystrophin-glycoprotein-complex, SGCG (y-sarcoglycan), 12 ITGB1 (12 -integrin tail), 17 SORBS1 (costamere-associated protein), 19 FBLIM1 (migfilin), 20 PGM5 (aciculin), 21 XIRPs (xin proteins; XIRP1, XIRP2), 21 SYNPO2 (synaptopodin 2), 22 MYOT (myotilin), 16 MYOZs (myozenins; MYOZ1, MYOZ2), 23 TTN (titin), 24 and HSP (heat shock proteins; HSPB1, 18 HSPB7 25).

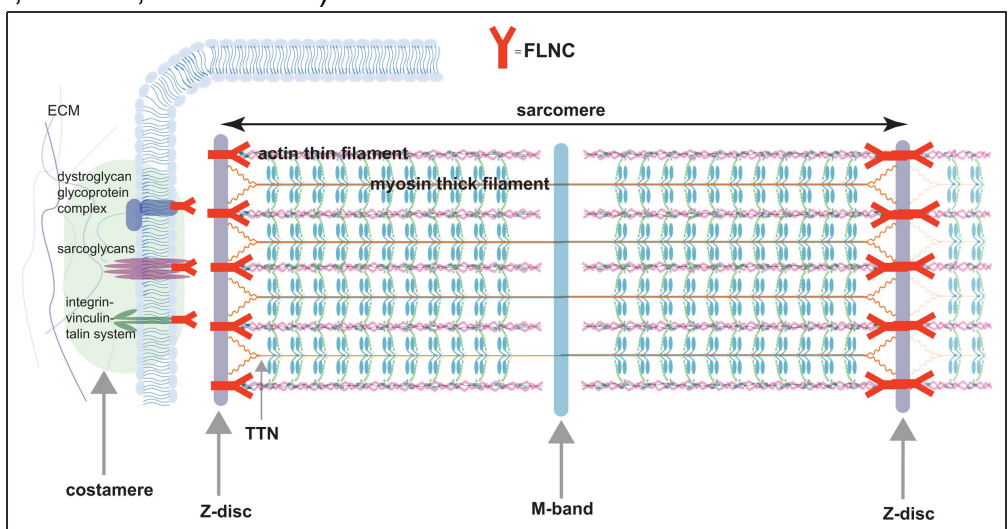


Figure 1. Sarcomere structure and FLNC (filamin C) localization in human induced pluripotent stem cell-derived cardiomyocytes. Schematic representation of the cardiac sarcomere, a highly-organized structure consisting of parallel arrays of thick and thin filaments. Myosin-rich (blue) thick filaments are anchored at the M-band and actin-rich (pink) thin filaments are anchored at Z-discs. FLNC (red) localizes primarily to Z-discs, where it crosslinks actin contained in thin filaments. Smaller amounts of FLNC also localize to costameres (light green oval), and intercalated discs (not shown). TTN (Titin) spans half of the sarcomere length extending from the Z-disc (N-terminus) to the M-band (C-terminus). ECM indicates extracellular matrix.

Homozygous ablation of *Flnc* in mice, flies, and fish produces abnormal Z-disc morphology, compromised sarcomere integrity, and striated muscle dysfunction.^{24,26–28} However, heterozygous *FLNC* variants in these model systems do not show overt striated muscle phenotypes, and thus their utility in understanding human cardiomyopathy pathogenesis has

remained limited. A related disease, myofibrillar myopathy (MFM), is also caused by truncating *FLNC* variants and shows large protein aggregates composed of FLNC and its binding partners in skeletal muscle.^{29,30} Although some patients with MFM also have DCM the converse is not true—the vast majority of DCM patients with pathogenic *FLNC* variants lack skeletal muscle involvement. Moreover, large protein aggregates are not reported in cardiac biopsies from *FLNC*-DCM patients.^{7,10} As such, the relatedness of pathogenic mechanisms involved in *FLNC* myofibrillar myopathy and *FLNC* cardiomyopathy remains unclear.

Here, we explored the mechanism of *FLNC* cardiomyopathy by employing CRISPR/Cas9 methodologies to produce and study a series of damaging *FLNC* variants in human induced pluripotent stem cell–derived cardiomyocytes (hiPSC-CMs). Unexpectedly, our studies reveal that homozygous and heterozygous *FLNC* variants have largely distinct consequences. From analyses of transcriptomic, proteomic, and live-cell imaging, we define a critical role for *FLNC* expression in sarcomere assembly and demonstrate proteopathic effects that ensue from heterozygous *FLNC* variants.

METHODS

Data Availability

The authors declare that all supporting data are available within the article (and its Data Supplement). Please see the Major Resources Table in the Data Supplement.

Culture and Maintenance of hiPSCs

PGP1 hiPSCs (derived from PGP1 donor from the Personal Genome Project) with an endogenous green florescent protein (GFP) tag on the sarcomere gene TTN^{31} were grown in Matrigel-coated 6-well tissue culture dishes, maintained in stem cell maintenance media (mTESR1, STEMCELL Technologies), and passaged every 2 to 3 days (passage range, 55–70) in the presence of 5 μ M ROCK (Rho kinase) inhibitor Y-27632 (125410; R&D Systems).

CRISPR/Cas9-Mediated Gene Editing of hiPSCs

The Benchling design tool was used for guideRNA and homology-directed repair arm design. Adherent hiPSCs were dissociated into single cells from the tissue culture plate using accutase, and nucleofected with 2 µg of Cas9 plasmid (pSpCas9[BB]-2A-Puro [PX459] V2.0, no. 62988; Addgene Plasmid), 4 µg of guideRNA pCR-BluntII-TOPO plasmid, and 4 µg of homology-directed repair arm using a Lonza nucleofector, as previously described.³² Edited colonies were subcloned and resequenced by MiSeq to confirm editing and population clonality.

Differentiation of hiPSC-CMs

hiPSCs seeded in Matrigel-coated 6-well culture plates were grown to 90% confluency for hiPSC-CM differentiation.³³ hiPSC-CMs were enriched by glucose deprivation at differentiation day 11 to 17. Unless indicated, all hiPSC-CMs were studied on or after day 30 to maximize cardiomyocyte maturity (eg, MYH7/MYH6 [myosin heavy chain] proteins=0.97±0.02).³⁴

Replating hiPSC-CMs for Imaging

hiPSC-CMs were dissociated and replated onto Matrigel-coated glass-bottom imaging-optimized 12-well plates (Mat-Tek) as described.³⁵

Contractility Analysis of hiPSC-CMs

Replated hiPSC-CMs were imaged as described³⁵ using a ×100 objective of a fluorescence microscope (Keyence BZ X-710) at an acquisition rate of 30 frames per second; sarcomere lengths and percent of sarcomere contraction were quantified using SarcTrack software.³⁶

Immunofluorescent Analyses of iPSC-CMs

Replated hiPSC-CMs were fixed, permeabilized, and stained with an F-actin molecular probe, FLNC (1:100, abcam Rb mAb, ab180941), TFEB (1:500, Cell Signaling Technology [CST], Rb mAb 37785), or NucBlue before imaging with a ×100 oil objective. For all immunofluorescent analyses, secondary antibody-only controls (abcam Rb [rabbit] monoclonalantibody ab150113, ab150116, ab150077, ab150080) were used to distinguish genuine target staining from background. Sarcomere content, anisotropy, and sarcomere persistence were quantified using custom MatLab algorithms (Extended Methods in the Data Supplement).

Patterning of hiPSC-CMs and Quantification of Sarcomere Striation

hiPSC-CMs were replated onto 2000 μm^2 fibronectin-coated rectangular polydimethylsiloxane micropatterns.³⁷ At 2 and 8 days after patterning, hiPSC-CMs were fixed, permeabilized, and stained with NucBlue and paxillin (610569, 1:100 dilution; BD Biosciences), and imaged using a $\times 100$ oil objective.

Live Imaging of Lysosomes in hiPSC-CMs

hiPSC-CMs were stained using 75 nM LysoTracker probe (LysoTracker Red DND-99, Thermo Fisher Scientific L7528) in RPMI B27 plus insulin media. Videos were acquired in an incubation chamber (37 °C, 5% CO₂) using a widefield fluorescence microscope (Keyence BZ X-710; ×100 objective, 30 frames/s). Lysosomes were also imaged using a ×100 objective of a spinning disk confocal microscope. Image data were processed using Fiji software.

Flow Cytometry of eGFP-TTN Expression in hiPSC-CMs

hiPSC-CMs were dissociated, strained through a 100 µm cell strainer, and eGFP signal was quantified with a FACSCanto flow cytometer. hiPSC-CMs without the eGFP-TTN tag were analyzed to set appropriate gates for the identification of GFP-TTN hiPSC-CMs. The resultant GFP (FITC-A) intensity frequency distributions were plotted using FlowJo software.

RNA Sequencing of hiPSC-CMs

Cells were lysed in Trizol Reagent (Life Technologies) for RNA extraction and stored at -80 °C until RNA was extracted. All RNA quality (RIN) and quantity were assessed on the TapeStation 2200 (Agilent) and all samples had an RNA integrity number (RIN) of >8. Library preparation was conducted using the Nextera library preparation method (Nextera XT DNA Library Preparation Kit, Illumina) and sequenced (Illumina NextSeq500 platform). All data were combined into a single

fastq file. Samples typically had 30M to 50M reads each. Seventy-five base pair-end reads were aligned to the human reference genome hg38 using Spliced Transcripts Alignment to a Reference. Raw reads were normalized to the total number of reads per kilobase of transcript per million.

Protein Isolation From Cell Lysates

hiPSC-CMs were washed and lysed with cold RIPA buffer containing protease and phosphatase inhibitors (Sigma-Aldrich 11873580001, Sigma-Aldrich 4906837001). To ensure lysis of nuclei, the lysate was passed 20× through a 21G needle, then shaken gently on ice for 15 minutes, and centrifuged (14 000*g* for 15 minutes). The supernatant was transferred to a fresh tube and protein concentration was quantified using the bicinchoninic assay kit (Pierce 23227).

Western Blotting

For each sample, 12.5 µg (or 20 µg for soluble/insoluble experiments) of protein lysate was loaded and resolved under denaturing conditions on a NuPAGE 3% to 8% Tris-Acetate Protein Gel (or 4%–20% Tris-Glycine Gel for soluble/insoluble and autophagic flux experiments). Proteins were wet transferred to a polyvinylidene fluoride (PVDF) membrane overnight at 40 mA at 4 °C or 70 V for 3 hours. Membrane was blocked for 1 hour at room temperature in 5% skim milk in TBST buffer, before addition of primary and secondary antibodies (Expanded Methods), and then imaged on an LI-COR Biosciences Odyssey CLx (infrared) or ChemiDoc BioRad imaging system.

Tandem-Mass-Tag Proteomics of hiPSC-CMs

Equal amounts of protein (≈100 μg) from each sample were digested into peptides for tandem-mass-tag quantitative proteome profiling as described.³⁸ Peptides were tagged with unique, sample-specific isobaric chemical labels (tandem-mass-tags) for multiplexing, and data were collected on an Orbitrap Fusion mass spectrometer in line with a Proxeon NanolC-1200 UHPLC. Database searching and reporter-ion quantification was performed using an in-house SEQUEST-based pipeline. To define relative abundance measurements, each protein was scaled such that the summed signal-to-noise for that protein across all channels was 100. Intensity-based absolute quantification values were used³⁹ to estimate absolute protein abundance using mass spectra processed using MaxQuant (Version 1.6.10.43). Otherwise, mass spectra were processed using a SEQUEST-based pipeline.³⁸ Protein quantification values were exported for further analysis in R (histograms, heatmaps, scatterplots) and bar graphs (GraphPad Prism).

Soluble/Insoluble Protein Fractionation of hiPSC-CMs

hiPSC-CMs protein lysates were fractionated into soluble and insoluble fractions using previously described methods.⁴⁰ Cells were washed with PBS and then lysed in ice-cold CellLytic M buffer (Sigma) containing protease inhibitors (Roche) for 30 minutes. The cells were centrifuged at 12 000*g* for 15 minutes and supernatants were collected, generating the soluble fraction. The pellets were dissolved in DNAse I (Roche), homogenized, and gently sonicated for 4 minutes, generating the insoluble fraction. Insoluble fractions were then used for Western blotting or mass spectrometry.

Autophagic Flux Analyses

hiPSC-CMs were washed 1X with PBS and cultured in either RPMI B27 plus insulin (fed) or DMEM minus glucose (starved) for 4 hours. Cells were treated with and without 400nM of bafilomycin A1 for 4 hours. Western blotting was used to determine the expression of LC3b-I, LC3b-II, (microtubule associated protein 1 light chain 3 beta) and TUBB (β-tubulin), and densitometric quantitation was performed using the ChemiDoc BioRad imaging system. The absolute difference in the LC3-IIb/TUBB ratio between bafilomycin-treated and untreated cells was used to compute autophagic flux.

Statistical Analyses

Statistical analyses were performed using nonparametric tests (Wilcoxon rank-sum tests), or Student t tests (2-sided, assuming similar variances) when the dataset was large and normally distributed. P<0.05 was considered statistically significant. For transcriptome and proteome-wide analyses, Benjamini-Hochberg corrections were applied for multiple comparisons with an α =0.05 after restricting the analyses by fold-change, as specified in the main text. To assess the effects of genotype on levels of particular sets of proteins (including endoplasmic reticulum [ER] proteins, autophagy proteins, FLNC interactors, and lysosome protein levels), linear mixed models were fitted with protein concentrations as the outcome variable and the interaction of genotype and marker protein as the fixed effect. To allow for correlated measurements between experiments, the replicate number was used as a random variable, and χ^2 values and P values are reported. For differential expression analyses, fold-change cutoffs were determined by varying the fold-change criteria and selecting a threshold at the inflection point of the resultant graph, such that the foldchange cutoff was neither too permissive nor too restrictive. DAVID functional annotation clustering was used to conduct enrichment analyses and the topmost significant functional categories were selected for display.41

For all figures that include representative images, the individual sample that best represented the group mean was selected.

RESULTS

CRISPR/Cas9 Genome Engineering of FLNC Mutant hiPSC Lines

FLNC variants were introduced via CRISPR/Cas9 into the hiPSC line PGP1, which contains an endogenous GFP tag on the N-terminus of the sarcomere protein titin (eGFP-TTN). We targeted exon 30, a region that encodes the 15th immunoglobulin domain (Figure 2A), and produced isogenic hiPSCs with wild-type (WT) or mutated FLNC sequences. To model human DCM variants, we introduced a heterozygous truncating variant ($FLNC^{+/-}$, Table). For comparison, we also produced cells that carry this variant on both alleles (*FLNC*^{-/-}, Table).

Table. FLNC RNA and Protein Levels From Replicates (n) of Independent Differentiations of WT and Mutant hiPSC-CMs, as Determined by RNAseq and Mass Spectrometry (Table view)

cell line	Coding sequence Δ	predicted protein sequence Δ	FLNC RNA (RPKM), (n)	FLNC protein (%WT), (n)
WT	WT	WT	283 (3)	100 (3)

cell line	Coding sequence Δ	predicted protein sequence Δ	FLNC RNA (RPKM), (n)	FLNC protein (%WT), (n)
FLNC ^{-/-}	c.5021_5022insT	p.Gly1674X	20* (3)	6±0.5 (4)
FLNC ^{+/-}	c.5021_5022insT	p.Gly1674X	93* (2)	47±5 (3)
FLNC ^{+/Δ7aa}	c.5002_5022del21	p.Val1668_Gly1674del	324 (2)	90±21 (2)
FLNCG1674S/G1674S	c.5020G>A	p.Gly1674Ser	249 (1)	111±10 (3)

RNA and protein quantities are displayed as mean, and mean±95% CI, respectively. FLNC indicates filamin C; hiPSC-CM, human induced pluripotent stem cell–derived cardiomyocytes; RNAseq, RNA sequencing; RPKM, reads per kilobase of transcript per million; and WT, wild-type.

* Nonsense-mediated decay of the mutant FLNC transcript.

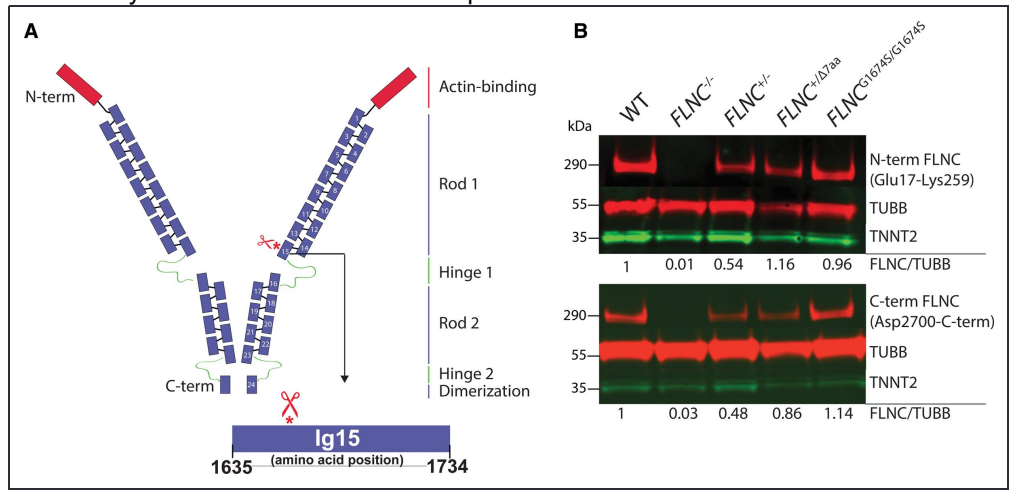


Figure 2. CRISPR/Cas9 genome engineering of filamin C (FLNC) mutant human induced pluripotent stem cell (hiPSC) lines and effects on FLNC expression in hiPSC-derived cardiomyocytes (hiPSC-CMs). A, Structure of FLNC, depicting an N-terminal (N-term) actin-binding domain (red) and 24 immunoglobulin (Ig)-like domains (blue). The CRISPR/Cas9 guide RNA targeted a cut site (scissors) in exon 30 (encoding the 15th Ig domain). B, Western blots of FLNC mutant hiPSC-CM protein extracts probed with N-term (top) and C-terminal (C-term; bottom) FLNC antibodies and loading controls TUBB (β -tubulin) and cardiac TNNT2 (troponin T). Numbers below blots indicate quantification of the relative intensity of FLNC to TUBB, normalized to wild-type (WT).

Spurious CRISPR mutagenesis also resulted in a heterozygous in-frame deletion of amino acids 1668-1674 ($FLNC^{+/\Delta7aa}$, Table). As FLNC in-frame insertion/deletions occur in patients with restrictive, hypertrophic, and dilated cardiomyopathies,^{3,10} we included $FLNC^{+/\Delta7aa}$ in our studies, recognizing that although not identified in patients, this variant had utility in understanding the fundamental biological mechanisms of mutant alleles that do not cause FLNC haploinsufficiency. We also produced and studied $FLNC^{G1674S/G1674S}$ cells. At the time, this study was initiated FLNC G1674S was a variant of unknown significance but has since been reclassified as likely benign given its high frequency (1.35×10⁻⁴) in the gnomAD (Genome Aggregation Database) database.⁴² As such, $FLNC^{G1674S/G1674S}$ hiPSC-CMs, which are isogenic to parental PGP1-derived CMs, serve as a control cell line.

Genotypes were confirmed with next-generation sequencing (Figure I in the Data Supplement). All lines differentiated into beating hiPSC-CMs, and principal component analyses of RNA sequencing profiles (Data Set I and Figure IIA in the Data Supplement) showed comparable degrees of maturity amongst all lines after 30 days of differentiation, with robust expression of prototypic cardiomyocyte genes, including *PLN*, *SERCA2A*, and *TTN* (Table I in the Data

Supplement).

Using tandem-mass-tag quantitative mass spectrometry-based proteomics, we studied replicates of WT and *FLNC* mutant hiPSC-CMs, where each replicate represents total cellular protein extracted from an independent differentiation. In an 8-plex experiment, we quantified the relative expression levels of 7123 proteins from WT (n=4) and $FLNC^{-/-}$ (n=4) hiPSC-CMs (Data Set II in the Data Supplement), and in an 11-plex experiment, we quantified 6863 proteins from WT (n=3), $FLNC^{+/-}$ (n=3), $FLNC^{+/\Delta 7aa}$ (n=2), and $FLNC^{G1674S/G1674S}$ (n=3) hiPSC-CMs (Data Set III in the Data Supplement). Hierarchical clustering analyses of protein expression data from the 8-plex and 11-plex tandem-mass-tag experiments showed appropriate clustering by genotype (Figure IIB and IIC in the Data Supplement).

Mass spectrometry of WT hiPSC-CMs identified over 100 FLNC peptides, which was significantly greater than the average number (≈8) of mapped peptides per protein, hinting that FLNC was abundantly expressed in hiPSC-CMs (Data Set IV in the Data Supplement). Intensity-based absolute quantification⁴³ estimated that FLNC was more abundant than 97.8% of proteins identified in hiPSC-CMs (Data Set IV in the Data Supplement).

Analysis of *FLNC* expression in WT and mutant hiPSC-CMs (Table) showed that $FLNC^{-/-}$ and $FLNC^{+/-}$ hiPSC-CMs had markedly reduced levels of *FLNC* transcript (7% and 33% of WT levels), likely reflecting mRNA nonsense-mediated decay. Mass spectrometry confirmed that FLNC protein levels were similarly reduced to 6% and 47% of WT, respectively (Table). By contrast, $FLNC^{+/\Delta7aa}$ and $FLNC^{G1674S/G1674S}$ hiPSC-CMs had FLNC transcript and protein levels comparable to WT cells (Table). Western blotting using N-terminal and C-terminal FLNC antibodies confirmed these findings (Figure 2B).

FLNC Is Necessary for Actin and Thin Filament Gene Expression and Sarcomere Assembly

Proteome-wide comparisons of WT and FLNC^{-/-} hiPSC-CMs (7123 total proteins) revealed 136 proteins that were differentially expressed (DE; Data Set II in the Data Supplement). Analyses of these DE proteins showed significant enrichment of actin-binding and sarcomere proteins (Table II in the Data Supplement). Parallel analyses of RNA sequencing data indicated that these decreased protein levels were largely attributable to reduced transcription, as there was a strong correlation between DE protein and transcript expression in FLNC^{-/-} hiPSC-CMs (r=0.91, Figure 3A). Included among these DE genes were the FLNC-binding partner synaptopodin (SYNPO), thin filament-associated sarcomere components (tropomyosin (TPM2), troponin I (TNN/3), and troponin T (TNNT1)), as well as Z-disc components (synaptopodin 2-like [SYNPO2L], ankyrin repeat domain 1 [ANKRD1], PDZ and LIM domain 3 [PDLIM3], leomodin 2 [LMOD2], cysteine and glycine-rich protein 3 [CSRP3]; Figure 3A). By contrast, proteins of the thick filament and M-band (TTN, MYBPC3, [myosin binding protein C] nebulette, MYOM1, MYOM2) were only minimally (>75% of WT level) or not significantly affected, although the ratios of MYH6/MYH7 and MYL7/MYL2 (myosin light chain) transcripts were >5-fold increased, reflecting transcriptional isoform switches that are frequently observed in states of cardiomyocyte stress⁴⁴ (Data Set I and II in the Data Supplement).

B

*MYH6

*MYH6

*GFP2TIN

Merce

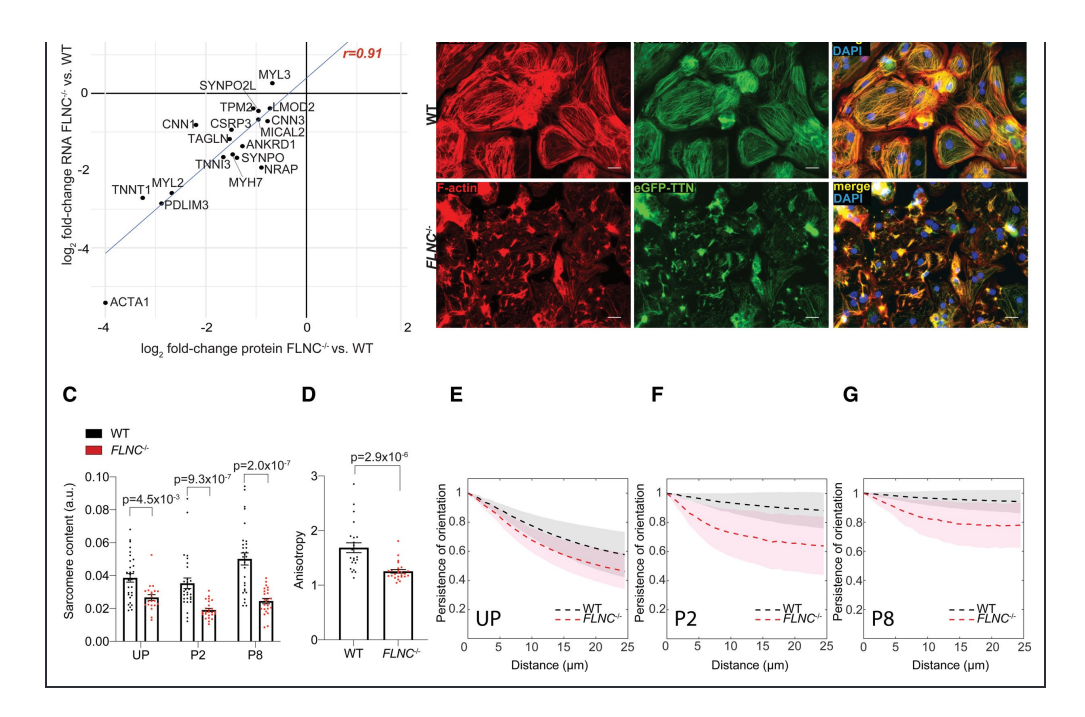


Figure 3. Impaired sarcomere and actin-related gene expression and deficient sarcomere assembly in FLNC^{-/-} human induced pluripotent stem cell-derived cardiomyocytes (hiPSC-CMs). A. Correlation (r=0.91) of sarcomere and actin-binding protein and RNA expression (quantified by mass spectrometry; wildtype (WT): n=4, FLNC^{-/-}: n=4 and RNA sequencing [RNAseq]; WT: n=3, FLNC^{-/-}: n=3). **B**, Costaining of F-actin (red) and eGFP-TTN (endogenous GFP titin; green, Z-discs) and DAPI (blue) in WT and FLNC-/hiPSC-CMs. Scale bar=25 μm. C, Sarcomere content of individual hiPSC-CMs on unpatterned (UP) surfaces and on micropatterned surfaces, quantified 2 (P2) and 8 (P8) d after replating (WT: n=20 [UP], 28 [P2], 30 [P8]; FLNC^{-/-}: n=21 [UP], 25 [P2], 25 [P8], Wilcoxon rank-sum tests). **D**, Anisotropic quantification of actin cytoskeletal organization from unpatterned images (WT: n=23, FLNC^{-/-} n=25, Wilcoxon rank-sum test). **E**, Persistence of sarcomere orientation in individual unpatterned hiPSC-CMs (WT: n=29, FLNC^{-/-}: n=21). **F**, Persistence of sarcomere orientation in individual patterned hiPSC-CMs 2 days postreplating (P2; WT: n=28, FLNC^{-/-}: n=25). **G**, Persistence of sarcomere orientation in individual patterned hiPSC-CMs 8 days postreplating (P8; WT: n=30, FLNC^{-/-}: n=21). For **E-G**, analyses were conducted on cells in the field of view from ≈10 representative images, and shaded area indicates SEM). ACTA indicates actin; ANKRD, ankyrin repeat domain containing; CNN, calponin; LMOD, leiomodin; MICAL, microtubule associated monooxygenase, calponin and LIM domain containing; MYH, myosin heavy chain; MYL, myosin light chain; NRAP, nebulin related anchoring protein; SYNPO (synaptopodin); TAGLN, transgelin; TNN, troponin; and TPM, tropomyosin.

Immunofluorescent analyses of actin and sarcomere structure in hiPSC-CMs (Figure 3B) showed that $FLNC^{-/-}$ hiPSC-CMs had significantly reduced sarcomere content (Figure 3C; mass spectrometry and flow cytometry showed comparable expression of eGFP-TTN in WT and $FLNC^{-/-}$ hiPSC-CMs (Figure IIIA and IIIB in the Data Supplement), thereby excluding an artifactual effect of the tagged TTN protein). $FLNC^{-/-}$ hiPSC-CMs also had disordered actin cytoskeletons (Figure 3B and 3D). Examination of individual replated cells also showed aberrant actin crosslinking in $FLNC^{-/-}$ hiPSC-CMs demonstrated by the marked size variation and breakage of actin bundles (Figure IIIC in the Data Supplement).

In our prior work, we demonstrated that sarcomere assembly and organization can often be promoted by culturing hiPSC-CMs on surfaces with micropatterned fibronectin matrices, which support the alignment of costameres with the ECM (extracellular matrix).³⁷ However, even when plated on micropatterned surfaces, *FLNC*^{-/-} hiPSC-CMs had reduced sarcomere content (Figure 3E through 3G, Figure IIID in the Data Supplement). Although these surfaces improved sarcomere

persistence, a metric of myofibril continuity, in both WT and $FLNC^{-/-}$ hiPSC-CMs, myofibrils in $FLNC^{-/-}$ hiPSC-CMs still remained less persistent compared with WT at both 2 and 8 days

 $FLNC^{-/-}$ hiPSC-CMs still remained less persistent compared with WT at both 2 and 8 days postreplating (Figure 3E through 3G). These studies indicate that even in the presence of an organized ECM, $FLNC^{-/-}$ hiPSC-CMs are unable to properly assemble and organize sarcomeres.

Despite severe deficits in sarcomere assembly, residual sarcomeres in *FLNC*^{-/-} hiPSC-CMs were still contractile (Movies I and II in the Data Supplement). However, these sarcomeres were significantly less contractile relative to WT, as assessed by high-throughput analysis of thousands of sarcomeres³⁶ (Figure 4, Data Set V in the Data Supplement). Many *FLNC*^{-/-} sarcomeres exhibited a conspicuous bending motion during cardiomyocyte relaxation (Movie III in the Data Supplement), a phase of the cardiac cycle when tropomyosin undergoes azimuthal movements to reposition it close to actin where electrostatic interactions maintain tropomyosin in a blocked state.⁴⁵ We suspect that inadequate actin crosslinking in *FLNC*^{-/-} hiPSC-CMs disrupted these movements and resulted in relaxation-dependent bending.

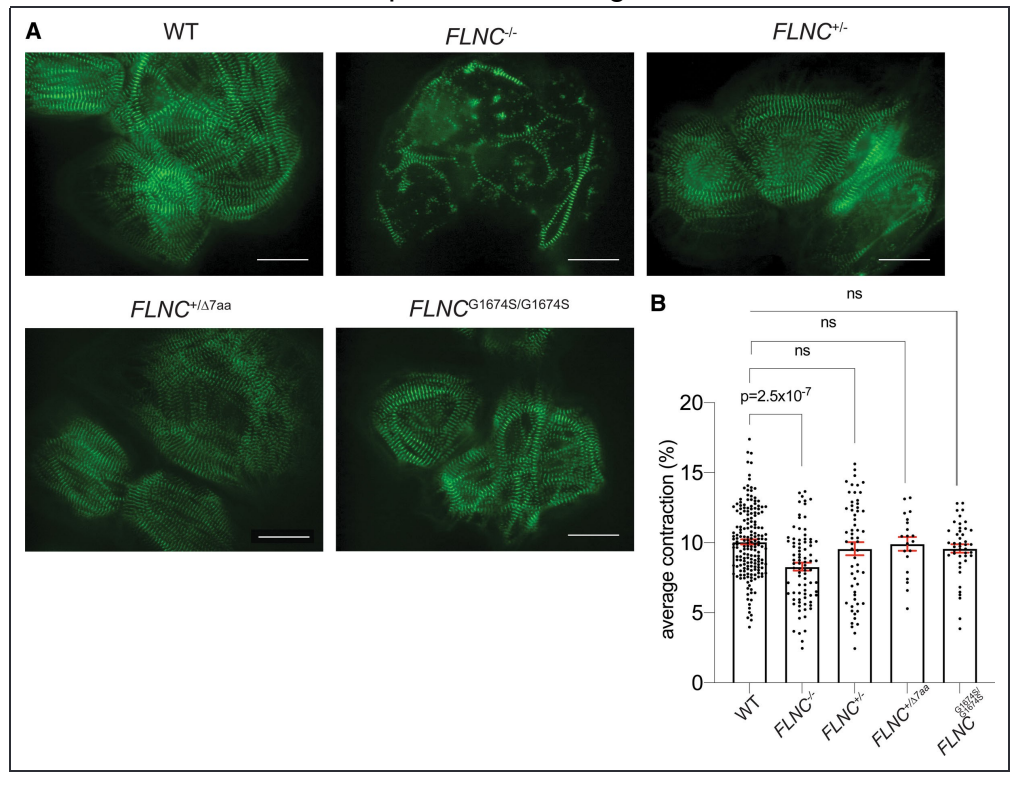


Figure 4. Sarcomere structure and function in FLNC mutant human induced pluripotent stem cell-derived cardiomyocytes (hiPSC-CMs). A, $FLNC^{-/-}$ hiPSC-CMs have fewer, often fragmented sarcomeres, whereas the other FLNC mutant lines assemble intact sarcomeres (eGFP-TTN [titin], green, Z-discs). Scale bar=25 μm. **B**, Sarcomere contractile function (average % shortening) in wild-type (WT) and FLNC mutant hiPSC-CMs, determined by SarcTrack high-throughput video analyses. Data are displayed as mean±SEM where each dot represents averaged sarcomere contraction percent calculated from one video. Data were gathered from multiple differentiations (n), videos (v), and total tracked sarcomeres (s) as follows: WT (n=6, v=181, s=47 498); $FLNC^{G1674S/G1674S}$ (n=2, v=44, s=12 934); $FLNC^{+/-}$ (n=3, v=59, s=13 006); $FLNC^{+/\Delta7aa}$ (n=2, v=20, s=3571); $FLNC^{-/-}$ (n=3, v=83, s=12 138). ns indicates nonsignificant.

Taken together, these studies of $FLNC^{-/-}$ hiPSC-CMs demonstrate multiple essential roles of FLNC in sarcomere biology including expression of a network of actin and thin filament genes, actin crosslinking at Z-discs, and maintenance of sarcomere structure during relaxation.

Distinct Abnormalities in hiPSC-CMs With Damaging Heterozygous FLNC **Variants**

Having identified impaired sarcomere structure, contractility, and relaxation in FLNC^{-/-} hiPSC-CMs, we expected similar defects in the heterozygous mutant lines. However, neither $FLNC^{+/-}$, FLNC^{+/Δ7aa} nor FLNC^{G1674S/G1674S} had significant changes in sarcomere structure or contractile performance in vitro (Figure 4, Movies IV through VI in the Data Supplement). Furthermore, unlike FLNC-/- hiPSC-CMs, the expression levels of most thin filament (TNNC1, TNNT2, TPM2) and thick filament (TTN, MYH6, MYH7, MYBPC3) proteins in these three lines were comparable to WT (Data Sets II and III in the Data Supplement).

To assess for other potentially pathogenic effects of these variants, we compared the entire proteomes (6863 proteins) of $FLNC^{+/-}$, $FLNC^{+/\Delta7aa}$, $FLNC^{G1674S/G1674S}$ and WT hiPSC-CMs. These proteome-wide analyses showed that FLNCG1674S/G1674S was indistinguishable from WT (Figure 5A), confirming G1674S as a benign variant and allowing its use as an additional independent control line. By contrast, $FLNC^{+/-}$ and $FLNC^{+/\Delta7aa}$ hiPSC-CMs had 212 and 568 DE proteins relative to WT (Data Set III in the Data Supplement); >50% of these DE proteins were shared by both $FLNC^{+/-}$ and $FLNC^{+/\Delta7aa}$ hiPSC-CMs, suggesting overlapping pathogenic effects (Figure 5A). The identity and expression patterns of DE proteins in $FLNC^{+/-}$ and $FLNC^{+/\Delta7aa}$ hiPSC-CMs were largely distinct from those of FLNC-/- hiPSC-CMs (Figure IVA in the Data Supplement), further implying that *FLNC* heterozygous alleles evoked different consequences than those caused by complete absence of FLNC.

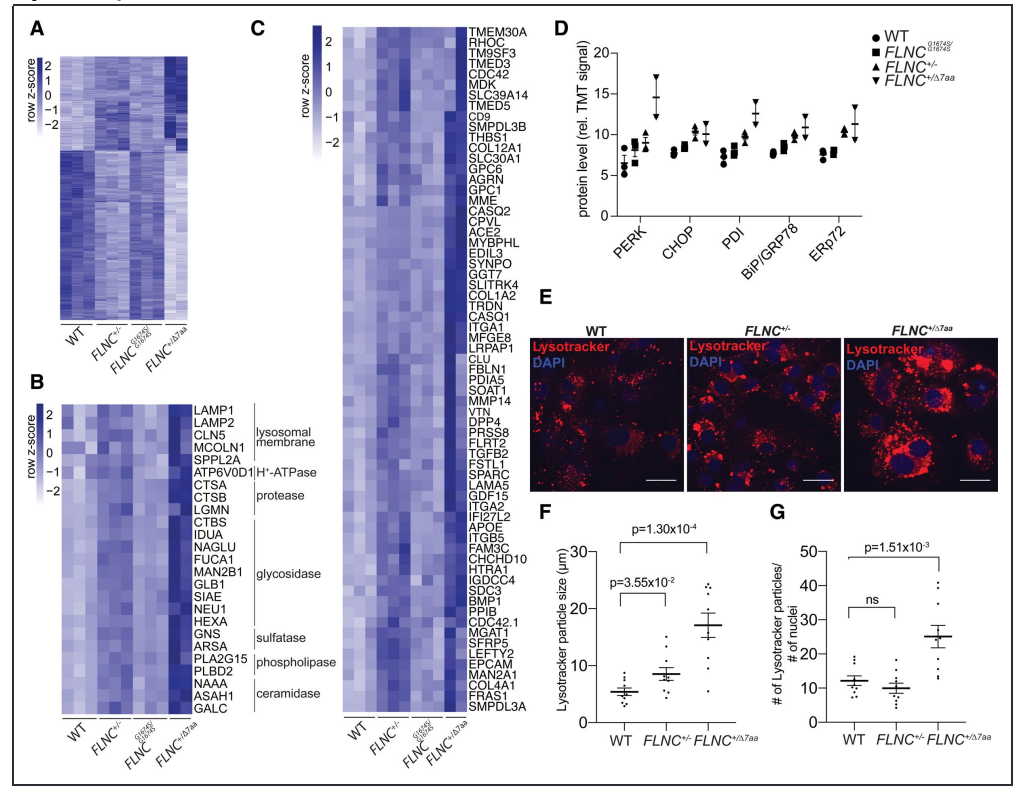


Figure 5. Damaging heterozygous FLNC variants in human induced pluripotent stem cell-derived cardiomyocytes (hiPSC-CMs) increase lysosome expression and cause intracellular accumulation of membrane and secreted proteins. A, From 6863 total proteins quantified by tandem-mass-tag mass spectrometry, differentially expressed (DE) proteins were identified in FLNC+/- (212 DE proteins), FLNC^{G1674S/G1674S} (0 DE proteins), and FLNC^{+/Δ7aa} hiPSC-CMs (568 DE proteins) relative to wild-type (WT;

DE: $\log_2[\text{fold-change}]|>0.67$ and Benjamini-Hochberg adjusted P<0.05). Three hundred fifty of these proteins were shared between $FLNC^{+/-}$ and $FLNC^{+/\Delta7aa}$ hiPSC-CMs (overlap criteria: $|\log_2(\text{fold-change})|>0.5$). Replicate columns in heatmap represent independent differentiations of each cell line (WT: n=3, $FLNC^{+/-}$: n=3, $FLNC^{G1674S/G1674S}$: n=3, $FLNC^{+/\Delta7aa}$: n=2). **B** and **C**, Row-scaled heatmaps of enriched protein groups (**B**: lysosome proteins, **C**: trafficked proteins). **D**, Endoplasmic reticulum markers are upregulated with increasing derangement in genotype from WT to $FLNC^{+\Delta7aa}$ (linear mixed model, $\chi^2=22.7$, P=0.0001). **E**, Representative confocal images of LysoTracker labeling (red) show increased lysosome content and clustering near nuclei (blue) in $FLNC^{+/-}$ and $FLNC^{+/\Delta7aa}$ hiPSC-CMs (scale bar=100 µm). **F**, Quantification of Lysotracker-stained particles, normalized to nuclear number (n=10 representative images per cell line, Wilcoxon rank-sum tests). **G**, Quantification of Lysotracker-stained particle size (WT: n=1869, $FLNC^{-/-}$: n=2055, $FLNC^{+/\Delta7aa}$: n=1910, where n=number of lysosomes quantitated from 10 representative images per cell line, Wilcoxon rank-sum tests). BiP/GRP78 indicates endoplasmic reticulum chaperone; CHOP, C/EBP-homologous protein 10; ERp72, protein disulfide isomerase family A member; ns, nonsignificant; PDI, prolyl hydroxylase subunit beta; and PERK, PRK-like ER kinase.

Among the 350 DE proteins shared between the $FLNC^{+/-}$ and $FLNC^{+/\Delta7aa}$ hiPSC-CMs, there was significant enrichment for lysosomal proteins (Table III in the Data Supplement, Figure 5B). Levels of lysosomal membrane proteins, as well as proteins that mediate lysosomal acidification, and lysosomal enzymes including proteases, glycosidases, sulfatases, phospholipases, and ceramidases were increased (Figure 5B). Neither $FLNC^{-/-}$ nor $FLNC^{G1674S/G1674S}$ hiPSC-CMs showed large changes in lysosomal protein expression (Figure IVB in the Data Supplement).

Additional enrichment was observed for proteins containing signal peptides, disulfide bonds, glycoproteins, and extracellular proteins in both $FLNC^{+/-}$ and $FLNC^{+/\Delta7aa}$ hiPSC-CMs (Table III in the Data Supplement, Figure 5C). As these terms reflect features of proteins that are destined for membrane incorporation or secretion, 46 we hypothesized that the increased abundance of these proteins within the cell could reflect ER stress and dysfunctional protein trafficking. Consistent with this hypothesis, $FLNC^{+/-}$ and $FLNC^{+/\Delta7aa}$ hiPSC-CMs had increased protein levels of ER stress markers including PERK (PRK-like ER kinase), CHOP (C/EBP homologous protein 10), PDI (prolyl 4-hydroxylase subunit beta), BiP/GRP78 (endoplasmic reticulum chaperone), and ERp72 (protein disulfide isomerase family A member 4), which infers activation of the PERK and ATF6 arms of the unfolded protein response (Figure 5D). 47 Involvement of the IRE-1 (inositol-requiring enzyme) arm of the unfolded protein response appeared minimal, as splicing of the XBP1 mRNA was not observed in either the WT or FLNC heterozygous cell lines (Figure IVC in the Data Supplement).

The levels of most lysosomal proteins, trafficked proteins, and ER stress markers were even higher in $FLNC^{+/\Delta7aa}$ than in $FLNC^{+/-}$ hiPSC-CMs (Figure 5B through 5D), inferring that the $\Delta7aa$ allele caused a similar, but more severe, cellular phenotype than that of the haploinsufficient allele.

Increased Lysosome Content in FLNC^{+/-} and FLNC^{+/Δ7aa} hiPSC-CMs

We considered whether increased lysosomal protein levels in $FLNC^{+/-}$ and $FLNC^{+/\Delta7aa}$ hiPSC-CMs reflected changes in organelle number or size. Using LysoTracker, a red fluorescent membrane-permeable dye that accumulates in acidic organelles, we directly visualized lysosomes in WT, $FLNC^{+/-}$, and $FLNC^{+/\Delta7aa}$ hiPSC-CMs (Figure 5E). Live-cell imaging showed active movement of Lysotracker-stained structures along linear paths in all cell lines (Movies VII through IX in the Data Supplement), indicating that these were appropriately acidic and dynamically motile along microtubules. Quantification of LysoTracker staining demonstrated that LysoTracker structures were significantly larger in $FLNC^{+/-}$ hiPSC-CMs and $FLNC^{+/\Delta7aa}$ (Figure 5F), as well as

more numerous in $FLNC^{+/\Delta7aa}$ relative to WT hiPSC-CMs (Figure 5G). Although the RNA and protein levels of TFEB (transcription factor EB), a master regulator of lysosomal biogenesis, ⁵⁰ were not significantly changed in $FLNC^{+/-}$ or $FLNC^{+/\Delta7aa}$ hiPSC-CMs (Figure VA in the Data Supplement), the proportion of nuclear to cytoplasmic TFEB was increased in $FLNC^{+/\Delta7aa}$ hiPSC-CMs relative to WT (Figure VB and VC in the Data Supplement), indicating TFEB activation. ^{51,52} Additionally, genes containing a Coordinated Lysosomal Expression and Regulation motif through which TFEB activates transcription ⁵⁰ had modest but significantly increased transcription in $FLNC^{+/-}$ and $FLNC^{+/\Delta7aa}$ hiPSC-CMs (Figure VD, Data Set I in the Data Supplement), suggesting that increased TFEB activity may have partially contributed to the increased expression of lysosomal genes, particularly in $FLNC^{+/\Delta7aa}$ hiPSC-CMs, although additional mechanisms are likely involved.

Increased Autophagic Flux and Altered Z-Disc Protein Handling in FLNC^{+/-} and FLNC^{+/-} and hiPSC-CMs

The increase in lysosome expression and abundance in $FLNC^{+/-}$ and $FLNC^{+/\Delta7aa}$ hiPSC-CMs suggested that autophagic pathways could be activated in these mutants. Consistent with this hypothesis, the levels of several autophagic proteins, including those involved in early phagophore formation (BECN1 [beclin-1], ATG13 [autophagy-related gene]), autophagosome formation (ATG2B, MAP1LC3A [microtubule associated protein 1 light chain 3 alpha], ATG7, ATG12, ATG5, ATG16L1), and regulators of autophagy including PRKACA and PRKACB^{53–55} were found in lower abundance in $FLNC^{+/-}$ and $FLNC^{+/\Delta7aa}$ compared with WT and $FLNC^{G1674S/G1674S}$ hiPSC-CMs (Figure 6A, Data Set III in the Data Supplement). We hypothesized that the depletion of these proteins reflected their consumption due to increased autophagic flux.

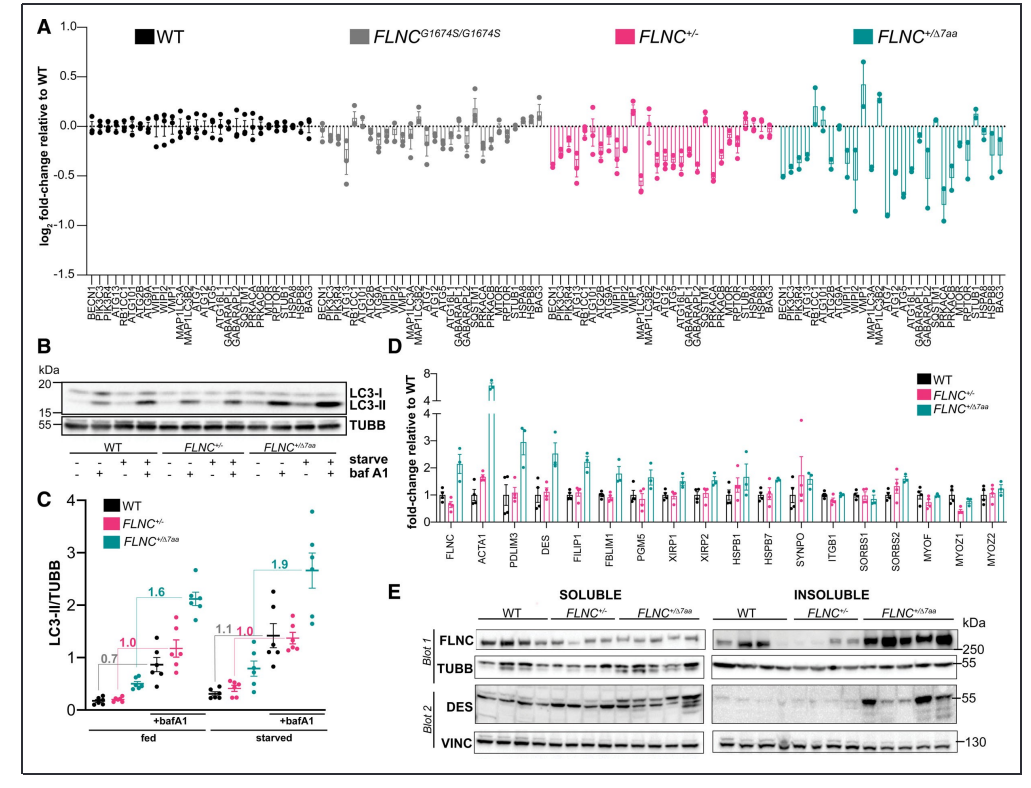


Figure 6. Heterozygous damaging FLNC variants cause depletion of autophagic proteins, increased autophagic flux, and accumulation of Z-disc proteins in human induced pluripotent stem cell-derived

cardiomyocytes (hiPSC-CMs). A, Levels of proteins involved in autophagy (including phagophore formation, autophagosome elongation, autophagosome maturation, regulation of autophagy) showing increasing derangement by genotype from FLNCG1674S/G1674S to FLNC+/Δ7aa hiPSC-CMs (linear mixed model, chisquared=271.6, P=3.2×10⁻⁴²). **B**, Representative Western blot showing LC3-I and LC3-II protein levels with TUBB (β-tubulin) as loading control. The relative difference in LC3-II/TUBB levels with and without Baf A1 (bafilomycin A1) was used to calculate autophagic flux under both fed and starved (glucose-depleted) conditions. C, Densitometric quantitation of LC3-II/TUBB normalized to total signal intensity per blot (n= 3 biological replicates × 2 technical replicates per genotype). Under both fed and starved conditions, the autophagic flux increases by genotype from wild-type (WT) to $FLNC^{+/\Delta7aa}$ (linear mixed model, $\chi^2=19.1$, $P=1.2\times10^{-5}$). The mean autophagic flux for each genotype is shown on plot. **D**, Quantitation of levels of FLNC and FLNC-interacting partners in insoluble protein fractions extracted from hiPSC-CMs by mass spectrometry (WT: n=4, $FLNC^{+/-}$: n=4, $FLNC^{+/\Delta7aa}$: n=3). $FLNC^{+/\Delta7aa}$ hiPSC-CMs show increased levels of FLNC and interacting partners in the insoluble fraction relative to WT (mean increase 88% [95% CI, 75%-100%], linear mixed model, P=8.6×10⁻⁵¹); FLNC^{+/-} hiPSC-CMs are not significantly affected. **E**, Western blot validation of enrichment of FLNC and DES (desmin) in the insoluble fraction of $FLNC^{+/\Delta7aa}$ relative to WT hiPSC-CMs (WT: n=4, $FLNC^{+/-}$: n=4, $FLNC^{+/\Delta7aa}$: n=5). TUBB indicates beta tubulin; and VINC, vinculin.

To measure autophagic flux, we assessed LC3b phosphatidylethanolamine conjugation in hiPSC-CMs cultured in both full and starvation (glucose-depleted) media (Figure 6B and 6C). Autophagic flux increased by genotype from WT to $FLNC^{+/-}$ to $FLNC^{+/-}$ to $FLNC^{+/-}$ hiPSC-CMs. This increase in flux by genotype was observed under both fed and starved conditions (Figure 6C). As autophagic flux was not significantly further upregulated by starvation in WT hiPSC-CMs, it is likely that 4 hours of glucose depletion was an insufficient stressor to result in a further increase in flux; nevertheless, the effect of genotype on flux is significant regardless of condition.

We hypothesized that the increase in lysosome content and autophagic flux in $FLNC^{+/-}$ and FLNC^{+/Δ7aa} hiPSC-CMs was triggered by protein aggregation of FLNC or other FLNC-binding partners. To test this hypothesis, total cellular protein from WT and FLNC mutant hiPSC-CMs was fractionated into soluble and insoluble fractions, and the insoluble fractions were subjected to analysis by mass spectrometry (Data Set VI in the Data Supplement). Analysis of FLNC-binding partners and associated Z-disc proteins showed that these proteins were enriched in the insoluble fractions of $FLNC^{+/\Delta7aa}$ hiPSC-CMs relative to WT (Figure 6D). The proteins with the greatest enrichment in $FLNC^{+/\Delta7aa}$ hiPSC-CMs included FLNC, striated muscle actin (ACTA1), PDLIM3 (PDZ and LIM Domain 3), DES (desmin), FILIP1 (FLNA interacting protein 1), and migfilin/FBLIM1 (FLN-binding LIM protein 1). The enrichment of these proteins in the insoluble fraction indicated that the FLNC^{Δ7aa} protein formed aggregates of FLNC and other FLNC-binding partners, similar to those that form with FLNC HCM missense variants. 9 Western blotting further confirmed the enrichment of FLNC and DES in the insoluble fractions of $FLNC^{+/\Delta7aa}$ hiPSC-CMs (Figure 6E). In contrast, FLNC^{+/-} hiPSC-CMs did not show significant enrichment of FLNC or its binding partners in the insoluble fraction relative to WT (Figure 6D and 6E; although FLNC+/- also carry only 50% of the amount of total FLNC protein).

Despite lacking enrichment of FLNC and FLNC-binding partners in the insoluble protein fraction, further analyses of total cellular lysate from $FLNC^{+/-}$ hiPSC-CMs showed significant accumulation of FLNC-binding partners and Z-disc proteins relative to WT (Figure VI, Data Set III in the Data Supplement); this accumulation was even greater in $FLNC^{+/\Delta 7aa}$ hiPSC-CMs compared to $FLNC^{+/-}$ hiPSC-CMs. Sarcomere proteins that were not part of the Z-disc including those of the thin (eg, TNNC1, TPM2) and thick filament (eg, MYH6, MYH7, MYBPC3) did not show

these effects (Figure VI in the Data Supplement). These data suggest that Z-disc protein turnover is modestly affected in $FLNC^{+/-}$ hiPSC-CMs, and more severely so in $FLNC^{+/\Delta7aa}$ hiPSC-CMs which form aggregates of FLNC and FLNC-binding proteins.

DISCUSSION

We demonstrate that FLNC is critical for sarcomere assembly and define the effects of damaging FLNC variants on cardiomyocyte biology (Figure 7). Complete loss of FLNC expression ($FLNC^{-/-}$) disrupted the coordinated expression of actin and thin filament genes, which reduced sarcomere content and impaired sarcomere function. FLNC haploinsufficiency ($FLNC^{+/-}$), a cause of DCM, did not disrupt sarcomere assembly and performance but rather impaired cardiomyocyte proteostasis, as reflected by the presence of ER stress, increased lysosome expression, and enhanced autophagic flux. Even more profound abnormalities in proteostasis occurred with an inframe deletion mutant encoding a misfolded FLNC protein ($FLNC^{+/\Delta7aa}$), which formed aggregates akin to those that accrue with damaging FLNC HCM missense variants.

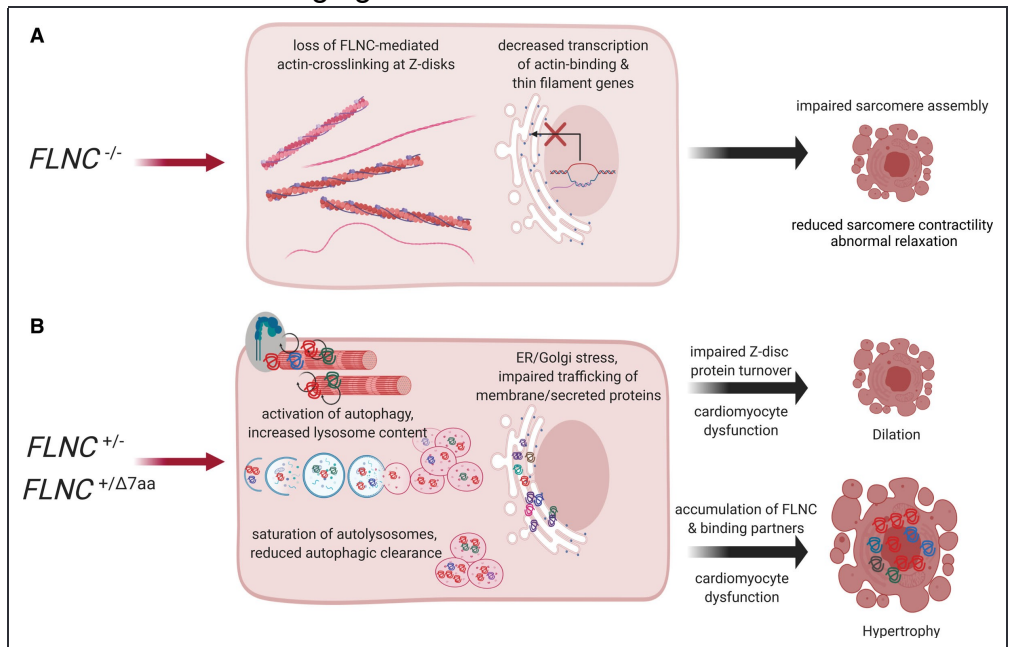


Figure 7. A model of the damaging effects of filamin C (*FLNC*) variants in human cardiomyocytes. A, Ablation of *FLNC* (*FLNC*^{-/-}) causes deficient actin crosslinking at Z-discs and inhibits transcription and translation of actin-related and sarcomere thin filament genes including *SYNPO*, *TPM2*, *TNNI3*, *TNNI3*, *SYNPO2L*, *ANKRD1*, *PDLIM3*, *LMOD2*, and *CSRP3*. This impairs sarcomere assembly, contractility, and relaxation in *FLNC*^{-/-} human induced pluripotent stem cell–derived cardiomyocytes. **B**, *FLNC* heterozygous variants disrupt sarcomere protein turnover at the Z-disc causing activation of autophagic clearance mechanisms and increases in lysosome content. Eventually, autophagic clearance mechanisms are overwhelmed and proteins begin to accumulate in the endoplasmic reticulum (ER)/Golgi, impairing the normal forward trafficking of sarcolemmal and secreted proteins. Variants that cause haploinsufficiency result in cardiac dilation and variants that cause misfolding and aggregation of FLNC and its binding partners result in hypertrophy. Made in ©Biorender: biorender.com.

The severe consequences of *FLNC* ablation on sarcomere structure in hiPSC-CMs are consistent with observations in other organisms and partially explained by the known role of FLNC in crosslinking actin at Z-discs.^{26,27} Surprisingly, *FLNC*^{-/-} hiPSC-CMs also failed to transcribe

(and translate) an entire network of sarcomere and actin-associated genes, including *SYNPO*, *TPM2*, *TNNI3*, *TNNT1*, *SYNPO2L*, *ANKRD1*, *PDLIM3*, *LMOD2*, and *CSRP3*. The disruption of RNA transcription of these genes indicates that *FLNC* has underappreciated roles in the coordinated regulation of the thin filament gene network. Ultimately, loss of FLNC-mediated actin crosslinking and deficient thin filament gene expression caused severe impairment of both contractility and relaxation in $FLNC^{-/-}$ hiPSC-CMs. These effects explain the embryonic lethality of homozygous null alleles in mice^{26,28} and the absence of homozygous null alleles in humans.⁴²

In contrast to $FLNC^{-/-}$ hiPSC-CMs, the sarcomere content, organization, and function of $FLNC^{+/-}$ hiPSC-CMs was indistinguishable from WT. Although experimental in vitro conditions cannot fully recapitulate in vivo mechanics and hemodynamics, the substantial differences between $FLNC^{-/-}$ and $FLNC^{+/-}$ hiPSC-CMs implied that haploinsufficiency evoked a different pathogenetic mechanism. The $FLNC^{+/\Delta7aa}$ mutant, which encoded a misfolded FLNC protein and shared >50% of DE proteins with $FLNC^{+/-}$ hiSPC-CMs, caused a similar but more profound cellular phenotype and was ultimately quite useful in elucidating abnormal proteostasis as a key disease mechanism for both heterozygous variants.

Proteomic analyses of insoluble protein fractions revealed that $FLNC^{+/\Delta7aa}$ hiPSC-CMs formed prominent aggregates of FLNC and its binding partners, akin to those that occur with FLNC missense alleles that also cause FLNC misfolding. Given its considerable abundance (top 3% of cardiomyocyte proteins), we suspect that aggregation of FLN imposes a profound burden on protein clearance mechanisms, which may evoke hypertrophic remodeling similar to other proteopathies such as cardiac amyloidosis. It is possible that the variable sequestration of particular FLNC-binding partners caused by distinct FLNC variants may contribute to the diversity of clinical phenotypes caused by FLNC variants.

Proteome-wide comparisons of the $FLNC^{+/\Delta 7aa}$ and $FLNC^{+/-}$ lines showed that $FLNC^{+/-}$ had a similar, although less severe phenotype than the $FLNC^{+/\Delta 7aa}$ hiPSC-CMs. Like $FLNC^{+/\Delta 7aa}$ hiPSC-CMs, $FLNC^{+/-}$ hiPSC-CMs also showed evidence of ER stress as well as increased lysosome content and autophagy, implying that the $FLNC^{+/-}$ variant also activated protein handling pathways. We suspect that the activation of protein handling pathways in the $FLNC^{+/-}$ and $FLNC^{+/\Delta 7aa}$ lines occurred by similar mechanisms induced by inefficient protein turnover at the Z-disc. The greater severity of phenotype in $FLNC^{+/\Delta 7aa}$ is likely secondary to the formation of aggregates of FLNC and a wide range of FLNC-binding partners in this mutant, which places an even greater burden on protein clearance pathways. However, $FLNC^{+/-}$ hiPSC-CMs produce half-normal levels of FLNC protein, and thus the accumulation of FLNC and its binding partners is likely more modest, resulting in an intermediate phenotype. Although our investigations suggest that both FLNC haploinsufficient and aggregate forming variants ultimately both cause proteotoxicity by similar mechanisms, one limitation of this study is that $FLNC^{+/\Delta 7aa}$ is not a clinical variant. Future studies will investigate whether other FLNC clinical missense and indel variants also produce proteotoxicity, as proposed by our model (Figure 7).

Our investigations add to a growing body of work that recognizes the importance of lysosomes in the turnover of Z-disc proteins. The central role of lysosomes in this process is highlighted by the profound cardiomyopathy that occurs with damaging variants in X-linked *LAMP2* which deplete the encoded lysosomal-associated membrane protein-2 and cause multisystem disease in affected

males.⁵⁷ Electrostimulation of soleus muscles isolated from *Lamp2*-null mice results in Z-disc disintegration—another indication that lysosome-mediated degradation is essential at the Z-disc.⁵⁸ The importance of lysosomes in Z-disc protein turnover may explain their accumulation with damaging heterozygous *FLNC* variants and also why lysosome content was not increased with homozygous null alleles, in which Z-disc and thin filament gene expression is inhibited. The downregulation of thin filament gene transcription in *FLNC*^{-/-} hiPSC-CMs suggests that cardiomyocytes may have intrinsic mechanisms to sense Z-disc stoichiometry and negatively regulate their transcription and assembly in the absence of key components such as FLNC, perhaps so as to prevent pathological protein aggregation. Further study of the mechanisms by which cardiomyocytes determine the stoichiometry of Z-disc protein complexes and then dispose of excess or damaged proteins in lysosomes is likely to provide further insights into the fundamental processes of sarcomere assembly and repair.

Impaired proteostasis is an emerging mechanism of cardiomyopathy that also occurs with pathogenic variants in other Z-disc genes including MYOT and DES, both of which, like FLNC, cause DCM and MFM.⁵⁹ Furthermore, loss of function variants in Z-disc chaperones also cause DCM and MFM. These include the DES chaperone, αβ-cystallin (CRYAB), 59,60 and the BAG domain-containing cochaperone (BAG3), which concentrates at Z-discs and cooperates with the autophagy adaptor protein, p62, to dispose of ubiquitinated FLNC.58 FLNC+/- hiPSC-CMs had depleted levels of two additional Z-disc chaperones—HSPB1 and HSPB7—both of which interact with FLNC and promote its proper localization and folding. 18,25 Loss of HSPB7 leads to FLNC aggregation, cardiomyocyte dysfunction, and myopathy in zebrafish, mice, and cultured human cardiomyocytes. 25,61,62 Replenishment of these critical Z-disc chaperone proteins, and further augmentation of protein handling pathways that are inadequate in FLNC+/- cardiomyocytes, may be broadly therapeutic for patients with Z-disc-related cardiac and skeletal myopathies. Additional interventions to increase autophagic flux through pharmacological modulation and lifestyle modifications, such as endurance exercise and caloric restriction, may also have clinical value. 63,64 hiPSC-CMs carrying FLNC variants provide an ideal model system to test the efficacy of these interventions.

In conclusion, damaging *FLNC* variants produce proteopathic cardiomyopathies and reinforce the critical roles for the lysosome-dependent turnover of excess, misfolded, or damaged proteins in cardiomyocytes. The growing recognition of pathological protein accumulation that occurs in many genetic and unsolved causes of DCM, HCM, and MFM indicates that an improved understanding of associated mechanisms and development of appropriate interventions has the potential to benefit many patients with these proteopathic myopathies.

ARTICLE INFORMATION

Received April 3, 2020; revision received August 6, 2021; accepted August 17, 2021; published online August 18, 2021.

The Data Supplement is available with this article at https://www.ahajournals.org/doi/suppl/10.1161/CIRCRESAHA.120.317076.

For Sources of Funding and Disclosures, see page 764.

Correspondence

Correspondence to: J.G Seidman, PhD, 77 Avenue Louis Pasteur, Boston, MA 02115. Email seidman@genetics.med.harvard.edu

Affiliations

Department of Genetics (R.A., C.N.T., Q.Z., J.G., S.R.D., C.E.S., J.G.S.), Harvard Medical School, Boston, MA. Department of Cell Biology(J.A.P., S.P.G.), Harvard Medical School, Boston, MA. Radcliffe Department of Medicine (C.N.T.), University of Oxford, United Kingdom. Wellcome Centre for Human Genetics (C.N.T.), University of Oxford, United Kingdom. Howard Hughes Medical Institute, Chevy Chase, MD (C.E.S.). Division of Genetics, Department of Medicine, Brigham and Women's Hospital, Boston, MA (C.E.S.). Department of Biomedical Engineering, Boston University, MA (J.K.E., S.S., A.C., C.S.C.). Wyss Institute for Biologically Inspired Engineering, Harvard University, Boston, MA (S.S., A.C., C.S.C.).

Acknowledgments

We thank the Harvard Medical School (HMS) Micron Core for assistance with cardiomyocyte imaging and the National Science Foundation (NSF) Engineering Research Center on Cellular Metamaterials (EEC-1647837) for expertise in patterning human induced pluripotent stem cell–derived cardiomyocytes (hiPSC-CMs). Graphics including graphical abstract were created with BioRender.com.

Sources of Funding

This work was supported in part by grants from the National Institutes of Health (NIH) National Heart Lung and Blood Institute (F30HL147389 to R. Agarwal), the NIH National Heart Lung and Blood Institute, and Leducq Foundation (HL084553 and HL080494 to J.G. Seidman and C.E. Seidman), the Howard Hughes Medical Institute (to C.E. Seidman), NIH National Institute of General Medical Sciences (R01 GM132129 to J.A. Paulo and GM97645 to S.P. Gygi), the British Heart Foundation Centre for Research Excellence award (RE/18/3/34214 to C.N. Toepfer), the National Science Foundation Graduate Research Fellowships Program (DGE-1840990 to J.K. Ewoldt), and the Sir Henry Wellcome Fellowship (206466/Z/17/Z to C.N. Toepfer).

Disclosures

C.E. Seidman and J.G. Seidman are founders and own shares in Myokardia Inc., a startup company that is developing therapeutics that target the sarcomere. C.N. Toepfer is a consultant for Myokardia Inc. The other authors report no conflicts.

SUPPLEMENTAL MATERIALS

Expanded Materials and Methods
Data Supplement Figures I–VI
Data Supplement Movies I–IX
Data Sets I–VI
References 31–39

REFERENCES

 Schultheiss HP, Fairweather D, Caforio ALP, Escher F, Hershberger RE, Lipshultz SE, Liu PP, Matsumori A, Mazzanti A, McMurray J, et al. Dilated cardiomyopathy. *Nat Rev Dis Primers*. 2019;5:32. doi: 10.1038/s41572-019-0084-1 Crossref. PubMed.

- 2. Cho KW, Lee J, Kim Y. Genetic variations leading to familial dilated cardiomyopathy. *Mol Cells*. 2016;39:722–727. doi: 10.14348/molcells.2016.0061 PubMed.
- 3. Ader F, De Groote P, Réant P, Rooryck-Thambo C, Dupin-Deguine D, Rambaud C, Khraiche D, Perret C, Pruny JF, Mathieu-Dramard M, et al. FLNC pathogenic variants in patients with cardiomyopathies: prevalence and genotype-phenotype correlations. *Clin Genet*. 2019;96:317–329. doi: 10.1111/cge.13594 Crossref. PubMed.
- 4. Begay, RL, Tharp, CA, Martin, A, Graw, SL, Sinagra, G, Miani, D, et al. HHS public access. 2017;1:344–359. doi: 10.1016/j.jacbts.2016.05.004.FLNC
- Janin A, N'Guyen K, Habib G, Dauphin C, Chanavat V, Bouvagnet P, Eschalier R, Streichenberger N, Chevalier P, Millat G. Truncating mutations on myofibrillar myopathies causing genes as prevalent molecular explanations on patients with dilated cardiomyopathy. *Clin Genet*. 2017;92:616–623. doi: 10.1111/cge.13043 Crossref. PubMed.
- Ortiz-Genga MF, Cuenca S, Dal Ferro M, Zorio E, Salgado-Aranda R, Climent V, Padrón-Barthe L, Duro-Aguado I, Jiménez-Jáimez J, Hidalgo-Olivares VM, et al. Truncating FLNC mutations are associated with high-risk dilated and arrhythmogenic cardiomyopathies. *J Am Coll Cardiol*. 2016;68:2440–2451. doi: 10.1016/j.jacc.2016.09.927 Crossref. PubMed.
- 7. Begay RL, Graw SL, Sinagra G, Asimaki A, Rowland TJ, Slavov DB, Gowan K, Jones KL, Brun F, Merlo M, et al. Filamin C truncation mutations are associated with arrhythmogenic dilated cardiomyopathy and changes in the cell–cell adhesion structures. *JACC: Clin Electrophysiol*. 2018;4:504–514. doi: 10.1016/j.jacep.2017.12.003 Crossref. PubMed.
- 8. Peters S, Kumar S, Elliott P, Kalman JM, Fatkin D. Arrhythmic genotypes in familial dilated cardiomyopathy: implications for genetic testing and clinical management. *Heart Lung Circ*. 2019;28:31–38. doi: 10.1016/j.hlc.2018.09.010 Crossref. PubMed.
- 9. Valdés-Mas R, Gutiérrez-Fernández A, Gómez J, Coto E, Astudillo A, Puente DA, Reguero JR, Álvarez V, Morís C, León D, et al. Mutations in filamin C cause a new form of familial hypertrophic cardiomyopathy. *Nature Commun.* 2014;5:1–9. doi: 10.1038/ncomms6326 Crossref.
- Verdonschot JAJ, Vanhoutte EK, Claes GRF, Helderman-van den Enden ATJM, Hoeijmakers JGJ, Hellebrekers DMEI, de Haan A, Christiaans I, Lekanne Deprez RH, Boen HM, et al. A mutation update for the FLNC gene in myopathies and cardiomyopathies. *Hum Mutat*. 2020;41:1091–1111. doi: 10.1002/humu.24004 Crossref. PubMed.
- Hartwig JH, Stossel TP. Structure of macrophage actin-binding protein molecules in solution and interacting with actin filaments. *J Mol Biol*. 1981;145:563–581. doi: 10.1016/0022-2836(81)90545-3 Crossref. PubMed.
- 12. Thompson TG, Chan YM, Hack AA, Brosius M, Rajala M, Lidov HG, McNally EM, Watkins S, Kunkel LM. Filamin 2 (FLN2): a muscle-specific sarcoglycan interacting protein. *J Cell Biol.* 2000;148:115–126. doi: 10.1083/jcb.148.1.115 Crossref. PubMed.
- 13. van der Flier A, Sonnenberg A. Structural and functional aspects of filamins. *Biochim Biophys Acta*. 2001;1538:99–117. doi: 10.1016/s0167-4889(01)00072-6 Crossref. PubMed.
- 14. Pudas R, Kiema TR, Butler PJ, Stewart M, Ylänne J. Structural basis for vertebrate filamin dimerization. *Structure*. 2005;13:111–119. doi: 10.1016/j.str.2004.10.014 Crossref. PubMed.
- 15. Razinia Z, Mäkelä T, Ylänne J, Calderwood DA. Filamins in mechanosensing and signaling. *Annu Rev Biophys*. 2012;41:227–246. doi: 10.1146/annurev-biophys-050511-102252 Crossref. PubMed.

- 16. van der Ven PF, Wiesner S, Salmikangas P, Auerbach D, Himmel M, Kempa S, Hayess K, Pacholsky D, Taivainen A, Schröder R, et al. Indications for a novel muscular dystrophy pathway. gamma-filamin, the muscle-specific filamin isoform, interacts with myotilin. *J Cell Biol*. 2000;151:235–248. doi: 10.1083/jcb.151.2.235 Crossref. PubMed.
- 17. Kiema T, Lad Y, Jiang P, Oxley CL, Baldassarre M, Wegener KL, Campbell ID, Ylänne J, Calderwood DA. The molecular basis of filamin binding to integrins and competition with talin. *Mol Cell*. 2006;21:337–347. doi: 10.1016/j.molcel.2006.01.011 Crossref. PubMed.
- 18. Collier MP, Alderson TR, de Villiers CP, Nicholls D, Gastall HY, Allison TM, Degiacomi MT, Jiang H, Mlynek G, Fürst DO, et al. HspB1 phosphorylation regulates its intramolecular dynamics and mechanosensitive molecular chaperone interaction with filamin C. Sci Adv. 2019;5:eaav8421. doi: 10.1126/sciadv.aav8421 Crossref. PubMed.
- Zhang M, Liu J, Cheng A, Deyoung SM, Saltiel AR. Identification of CAP as a costameric protein that interacts with filamin C. *Mol Biol Cell*. 2007;18:4731–4740. doi: 10.1091/mbc.e07-06-0628 Crossref. PubMed.
- 20. Tu Y, Wu S, Shi X, Chen K, Wu C. Migfilin and Mig-2 link focal adhesions to filamin and the actin cytoskeleton and function in cell shape modulation. *Cell.* 2003;113:37–47. doi: 10.1016/s0092-8674(03)00163-6 Crossref. PubMed.
- 21. Molt S, Bührdel JB, Yakovlev S, Schein P, Orfanos Z, Kirfel G, Winter L, Wiche G, van der Ven PF, Rottbauer W, et al. Aciculin interacts with filamin C and Xin and is essential for myofibril assembly, remodeling and maintenance. *J Cell Sci.* 2014;127:3578–3592. doi: 10.1242/jcs.152157 PubMed.
- 22. Linnemann A, van der Ven PF, Vakeel P, Albinus B, Simonis D, Bendas G, Schenk JA, Micheel B, Kley RA, Fürst DO. The sarcomeric Z-disc component myopodin is a multiadapter protein that interacts with filamin and alpha-actinin. *Eur J Cell Biol.* 2010;89:681–692. doi: 10.1016/j.ejcb.2010.04.004 Crossref. PubMed.
- 23. Takada F, Woude DLV, Tong H, Thompson TG, Watkins SC, Kunkel LM, Beggs AH. Myozenin: an alphaactinin and gamma-filamin-binding protein of skeletal muscle Z lines. *Proc Natl Acad Sci USA*. 2001;98:1595–1600. doi: 10.1073/pnas.041609698 PubMed.
- 24. González-Morales N, Holenka TK, Schöck F. Filamin actin-binding and titin-binding fulfill distinct functions in Z-disc cohesion. *PLoS Genet*. 2017;13:e1006880. doi: 10.1371/journal.pgen.1006880 Crossref. PubMed.
- 25. Juo LY, Liao WC, Shih YL, Yang BY, Liu AB, Yan YT. HSPB7 interacts with dimerized FLNC and its absence results in progressive myopathy in skeletal muscles. *J Cell Sci.* 2016;129:1661–1670. doi: 10.1242/jcs.179887 PubMed.
- Dalkilic I, Schienda J, Thompson TG, Kunkel LM. Loss of FilaminC (FLNc) results in severe defects in myogenesis and myotube structure. *Mol Cell Biol*. 2006;26:6522–6534. doi: 10.1128/MCB.00243-06 Crossref. PubMed.
- 27. Fujita M, Mitsuhashi H, Isogai S, Nakata T, Kawakami A, Nonaka I, Noguchi S, Hayashi YK, Nishino I, Kudo A. Filamin C plays an essential role in the maintenance of the structural integrity of cardiac and skeletal muscles, revealed by the medaka mutant zacro. *Dev Biol.* 2012;361:79–89. doi: 10.1016/j.ydbio.2011.10.008 Crossref. PubMed.
- 28. Yangzhao Z, Ze'e C, Lunfeng Z, Mason Z, Changming T, Xinmin Z, Sylvia ME, Xi F, Wei F, Ju C. Loss of filamin C is catastrophic for heart function. *Circulation*. 2020;141:869–871. doi: 10.1161/CIRCULATIONAHA.119.044061 Crossref. PubMed.

- 29. Vorgerd M, van der Ven PF, Bruchertseifer V, Löwe T, Kley RA, Schröder R, Lochmüller H, Himmel M, Koehler K, Fürst DO, et al. A mutation in the dimerization domain of filamin c causes a novel type of autosomal dominant myofibrillar myopathy. *Am J Hum Genet*. 2005;77:297–304. doi: 10.1086/431959 Crossref. PubMed.
- 30. Kley RA, Serdaroglu-Oflazer P, Leber Y, Odgerel Z, van der Ven PF, Olivé M, Ferrer I, Onipe A, Mihaylov M, Bilbao JM, et al. Pathophysiology of protein aggregation and extended phenotyping in filaminopathy. *Brain*. 2012;135:2642–2660. doi: 10.1093/brain/aws200 Crossref. PubMed.
- 31. Sharma A, Toepfer CN, Ward T, Wasson L, Agarwal R, Conner DA, Hu JH, Seidman CE. CRISPR/Cas9-mediated fluorescent tagging of endogenous proteins in human pluripotent stem cells. *Curr Protoc Hum Genet*. 2018;96:21.11.1-21.11.20. doi: 10.1002/cphg.52 Crossref.
- 32. Yang L, Yang JL, Byrne S, Pan J, Church GM. CRISPR/Cas9-directed genome editing of cultured cells. *Curr Protoc Mol Biol.* 2014;2014:31.1.1–31.1.17. doi: 10.1002/0471142727.mb3101s107
- 33. Lian X, Zhang J, Azarin SM, Zhu K, Hazeltine LB, Bao X, Hsiao C, Kamp TJ, Palecek SP. Directed cardiomyocyte differentiation from human pluripotent stem cells by modulating Wnt/β-catenin signaling under fully defined conditions. *Nat Protoc*. 2013;8:162–175. doi: 10.1038/nprot.2012.150 Crossref. PubMed.
- 34. Toepfer CN, Garfinkel AC, Venturini G, Wakimoto H, Repetti G, Alamo L, Sharma A, Agarwal R, Ewoldt JF, Cloonan P, et al. Myosin sequestration regulates sarcomere function, cardiomyocyte energetics, and metabolism, informing the pathogenesis of hypertrophic cardiomyopathy. *Circulation*. 2020;141:828–842. doi: 10.1161/CIRCULATIONAHA.119.042339 Crossref. PubMed.
- 35. Sharma A, Toepfer CN, Schmid M, Garfinkel AC, Seidman CE. Differentiation and contractile analysis of GFP-sarcomere reporter hiPSC-cardiomyocytes. *Curr Protoc Hum Genet*. 2018;96:21.12.1–21.12.12. doi: 10.1002/cphg.53 Crossref.
- 36. Toepfer CN, Sharma A, Cicconet M, Garfinkel AC, Mücke M, Neyazi M, Willcox JAL, Agarwal R, Schmid M, Rao J, et al. SarcTrack an adaptable software tool for efficient large-scale analysis of sarcomere function in hiPSC-cardiomyocytes. *Circ Res.* 2019;124:1172–1183. doi: 10.1161/CIRCRESAHA.118.314505 Crossref. PubMed.
- 37. Chopra A, Kutys ML, Zhang K, Polacheck WJ, Sheng CC, Luu RJ, Eyckmans J, Hinson JT, Seidman JG, Seidman CE, et al. Force generation via β-cardiac myosin, titin, and α-actinin drives cardiac sarcomere assembly from cell-matrix adhesions. *Dev Cell*. 2018;44:87–96.e5. doi: 10.1016/j.devcel.2017.12.012 Crossref. PubMed.
- 38. Navarrete-Perea J, Yu Q, Gygi SP, Paulo JA. Streamlined Tandem Mass Tag (SL-TMT) protocol: an efficient strategy for quantitative (phospho)proteome profiling using tandem mass tag-synchronous precursor selection-MS3. *J Proteome Res.* 2018;17:2226–2236. doi: 10.1021/acs.jproteome.8b00217 Crossref. PubMed.
- 39. Schwanhäusser B, Busse D, Li N, Dittmar G, Schuchhardt J, Wolf J, Chen W, Selbach M. Global quantification of mammalian gene expression control. *Nature*. 2011;473:337–342. doi: 10.1038/nature10098 Crossref. PubMed.
- 40. Xu N, Gulick J, Osinska H, Yu Y, McLendon PM, Shay-Winkler K, Robbins J, Yutzey KE. Ube2v1 positively regulates protein aggregation by modulating ubiquitin proteasome system performance partially through K63 ubiquitination. *Circ Res.* 2020;126:907–922. doi: 10.1161/CIRCRESAHA.119.316444 Crossref. PubMed.

- 41. Huang da W, Sherman BT, Lempicki RA. Systematic and integrative analysis of large gene lists using DAVID bioinformatics resources. *Nat Protoc.* 2009;4:44–57. doi: 10.1038/nprot.2008.211 Crossref. PubMed.
- 42. Karczewski KJ, Francioli LC, Tiao G, Cummings BB, Alföldi J, Wang Q, Collins RL, Laricchia KM, Ganna A, Birnbaum DP, et al; Genome Aggregation Database Consortium. The mutational constraint spectrum quantified from variation in 141,456 humans. *Nature*. 2020;581:434–443. doi: 10.1038/s41586-020-2308-7 Crossref. PubMed.
- 43. Arike L, Valgepea K, Peil L, Nahku R, Adamberg K, Vilu R. Comparison and applications of label-free absolute proteome quantification methods on Escherichia coli. *J Proteomics*. 2012;75:5437–5448. doi: 10.1016/j.jprot.2012.06.020 Crossref. PubMed.
- 44. Harvey PA, Leinwand LA. Cellular mechanisms of cardiomyopathy. *JCB: Rev.* 2011;194:355–365. doi: 10.1083/jcb.201101100 Crossref. PubMed.
- 45. Kiani FA, Lehman W, Fischer S, Rynkiewicz MJ. Spontaneous transitions of actin-bound tropomyosin toward blocked and closed states. *J Gen Physiol*. 2018;151:4–8. doi: 10.1085/jgp.201812188 Crossref. PubMed.
- 46. Feige MJ, Hendershot LM. Disulfide bonds in ER protein folding and homeostasis. *Curr Opin Cell Biol.* 2011;23:167–175. doi: 10.1016/j.ceb.2010.10.012 Crossref. PubMed.
- 47. Gardner BM, Pincus D, Gotthardt K, Gallagher CM, Walter P. Endoplasmic reticulum stress sensing in the unfolded protein response. *Cold Spring Harb Perspect Biol.* 2013;5:a013169. doi: 10.1101/cshperspect.a013169 Crossref. PubMed.
- 48. Uemura A, Oku M, Mori K, Yoshida H. Unconventional splicing of XBP1 mRNA occurs in the cytoplasm during the mammalian unfolded protein response. *J Cell Sci.* 2009;122:2877–2886. doi: 10.1242/jcs.040584 Crossref. PubMed.
- 49. Guardia CM, Farías GG, Jia R, Pu J, Bonifacino JS. BORC functions upstream of kinesins 1 and 3 to coordinate regional movement of lysosomes along different microtubule tracks. *Cell Rep.* 2016;17:1950–1961. doi: 10.1016/j.celrep.2016.10.062 Crossref. PubMed.
- 50. Sardiello M, Palmieri M, di Ronza A, Medina DL, Valenza M, Gennarino VA, Di Malta C, Donaudy F, Embrione V, Polishchuk RS, et al. A gene network regulating lysosomal biogenesis and function. *Science*. 2009;325:473–477. doi: 10.1126/science.1174447 Crossref. PubMed.
- 51. Settembre C, Zoncu R, Medina DL, Vetrini F, Erdin S, Erdin S, Huynh T, Ferron M, Karsenty G, Vellard MC, et al. A lysosome-to-nucleus signalling mechanism senses and regulates the lysosome via mTOR and TFEB. *EMBO J.* 2012;31:1095–1108. doi: 10.1038/emboj.2012.32 Crossref. PubMed.
- 52. Medina DL, Di Paola S, Peluso I, Armani A, De Stefani D, Venditti R, Montefusco S, Scotto-Rosato A, Prezioso C, Forrester A, et al. Lysosomal calcium signalling regulates autophagy through calcineurin and TFEB. *Nat Cell Biol.* 2015;17:288–299. doi: 10.1038/ncb3114 Crossref. PubMed.
- 53. Dikic I, Elazar Z. Mechanism and medical implications of mammalian autophagy. *Nat Rev Mol Cell Biol.* 2018;19:349–364. doi: 10.1038/s41580-018-0003-4 Crossref. PubMed.
- 54. Pohl C, Dikic I. Cellular quality control by the ubiquitin-proteasome system and autophagy. *Science*. 2019;366:818–822. doi: 10.1126/science.aax3769 Crossref. PubMed.
- 55. Stephan JS, Yeh Y, Ramachandran V, Deminoff SJ, Herman PK. The Tor and PKA signaling pathways independently target the Atg1 / Atg13 protein kinase complex to control autophagy. *Proc Natl Acad Sci USA*. 2009;106:17049–17054. doi: 10.1073/pnas.0903316106 Crossref. PubMed.

- 56. Bistola V, Parissis J, Foukarakis E, Valsamaki PN, Anastasakis A, Koutsis G, Efthimiadis G, Kastritis E. Practical recommendations for the diagnosis and management of transthyretin cardiac amyloidosis. *Heart Fail Rev.* 2021;26:861–879. doi: 10.1007/s10741-020-10062-w Crossref. PubMed.
- 57. Samad F, Jain R, Jan MF, Sulemanjee NZ, Menaria P, Kalvin L, Bush M, Jahangir A, Khandheria BK, Tajik AJ. Malignant cardiac phenotypic expression of Danon disease (LAMP2 cardiomyopathy). *Int J Cardiol*. 2017;245:201–206. doi: 10.1016/j.ijcard.2017.06.031 Crossref. PubMed.
- 58. Arndt V, Dick N, Tawo R, Dreiseidler M, Wenzel D, Hesse M, Fürst DO, Saftig P, Saint R, Fleischmann BK, et al. Chaperone-assisted selective autophagy is essential for muscle maintenance. *Curr Biol.* 2010;20:143–148. doi: 10.1016/j.cub.2009.11.022 Crossref. PubMed.
- 59. McLendon PM, Robbins J. Desmin-related cardiomyopathy: an unfolding story. *Am J Physiol Heart Circ Physiol*. 2019;3:1220–1228. doi: 10.1152/ajpheart.00601.2011
- 60. Tannous P, Zhu H, Johnstone JL, Shelton JM, Rajasekaran NS, Benjamin IJ, Nguyen L, Gerard RD, Levine B, Rothermel BA, et al. Autophagy is an adaptive response in desmin-related cardiomyopathy. *Proc Natl Acad Sci USA*. 2008;105:9745–9750. doi: 10.1073/pnas.0706802105 Crossref. PubMed.
- 61. Wu T, Mu Y, Bogomolovas J, Fang X, Veevers J, Nowak RB, Pappas CT, Gregorio CC, Evans SM, Fowler VM, et al. HSPB7 is indispensable for heart development by modulating actin filament assembly. *Proc Natl Acad Sci USA*. 2017;114:11956. doi: 10.1073/pnas.1713763114 Crossref.
- 62. Mercer EJ, Lin YF, Cohen-Gould L, Evans T. Hspb7 is a cardioprotective chaperone facilitating sarcomeric proteostasis. *Dev Biol.* 2018;435:41–55. doi: 10.1016/j.ydbio.2018.01.005 Crossref. PubMed.
- 63. Gámez A, Yuste-Checa P, Brasil S, Briso-Montiano Á, Desviat LR, Ugarte M, Pérez-Cerdá C, Pérez B. Protein misfolding diseases: prospects of pharmacological treatment. *Clin Genet*. 2018;93:450–458. doi: 10.1111/cge.13088 Crossref. PubMed.
- 64. Galluzzi L, Bravo-San Pedro JM, Levine B, Green DR, Kroemer G. Pharmacological modulation of autophagy: therapeutic potential and persisting obstacles. *Nat Rev Drug Discov*. 2017;16:487–511. doi: 10.1038/nrd.2017.22 Crossref. PubMed.

Novelty and Significance

What Is Known?

- Dominant heterozygous variants in filamin C (FLNC) can cause diverse cardiomyopathies.
- FLNC is a muscle-specific member of the class of actin crosslinking filamin proteins that is expressed primarily at sarcomere Z-discs.
- FLNC homozygous variants that cause loss of FLNC protein expression result in early lethality.
- FLNC heterozygous variants cause diverse forms of human cardiomyopathy with missense variants most often associated with hypertrophy and truncating variants most often associated with dilation.

What New Information Does This Article Contribute?

 FLNC homozygous variants profoundly impair sarcomere assembly and thin filament gene expression in human induced pluripotent stem cell—derived cardiomyocytes.

 Diverse FLNC heterozygous variants including those that cause haploinsufficiency and those that cause FLNC misfolding impair the turnover of Z-disc proteins, activate autophagy, and increase lysosome content in human induced pluripotent stem cell-derived cardiomyocytes.

Dominant heterozygous variants in *FLNC* cause diverse presentations of cardiomyopathy. Complete ablation of FLNC expression ($FLNC^{-/-}$) in human induced pluripotent stem cell–derived cardiomyocytes causes profound impairment of sarcomere assembly and thin filament gene expression. Human induced pluripotent stem cell–derived cardiomyocytes bearing *FLNC* heterozygous variants assemble sarcomeres but increase lysosome content and activate protein handling pathways due to impaired turnover of Z-disc proteins ($FLNC^{+/-}$, $FLNC^{+/\Delta 7aa}$) and protein aggregation of FLNC and its binding partners ($FLNC^{+/\Delta 7aa}$). Therapies to facilitate the appropriate degradation and disposal of accumulating Z-disc proteins may help antagonize cardiomyopathy progression caused by *FLNC* variants.